CrossMark

INVITED FEATURE PAPER

Thermodynamic limitations for alkali metals in $Cu(In,Ga)Se_2$

Dimitrios Hariskos[a] and Michael Powalla
Center for Solar Energy and Hydrogen Research Baden-Württemberg, Stuttgart 70563, Germany

(Received 21 July 2017; accepted 12 September 2017)

The efficiency of $Cu(In,Ga)Se_2$ (CIGS)-based solar cells could be continuously increased up to 22.6% by employing alkali metal dopants like Na, K, Rb, and Cs. The alkali metals are supplied to the CIGS layer from the glass substrate during deposition, from precursor layers or by a post deposition treatment. The alkali metal distribution in CIGS is not homogenous. Independently of the alkali metals used, their concentration at grain boundaries is much higher than that inside the grains. In this contribution, we discuss thermodynamic limitations for alkali metals in CIGS and show that in higher concentrations they are responsible for secondary phase separation. Applying the concept of immiscibility of phases for alkali metals in CIGS, we suggest how segregation at grain boundaries, formation of clusters in CIGS grains, sporadic formation of microstructures in the CIGS layer (hotspots, nodules), and separation of secondary phases with ordered structures can be interpreted.

I. INTRODUCTION

$Cu(In,Ga)Se_2$-(CIGS) or $Cu(In,Ga)(S,Se)_2$-(CIGSS)-based solar cell devices achieve laboratory scale conversion efficiencies up to 22.6%[1] for small-area cells and 19.2%[2] for 30 × 30 cm^2 submodules. On the industrial scale, commercial full-size modules reach efficiencies up to 17%[3] based on the total area of around 1 m^2.

Several methods have been developed for deposition of the chalcopyrite thin-film absorber layer. However, two approaches have become established for commercial manufacturing: the simultaneous evaporation of the elements (co-evaporation process) and the selenization or sulfoselenization of metallic precursor layers in a sequential two-step process (sequential process). The historical development of the CIGS technology and comparisons of different technologies and material properties is described in detail in different review articles[4–6] and books.[7–9]

The efficiency evolution of small-area devices since 1989 as extracted from the NREL's efficiency chart[10] is presented in Fig. 1. The progress made in the last three decades can be roughly divided into three periods.

In the first half of the 1990s, the developments in the co-evaporation process were dominated by a bilayer growth process[11,12] and the incorporation of Ga[13] for increasing the energy band gap for better adjustment to the solar spectrum. At the same time, the sequential process was generally based on the ARCO Solar process[14,15] by selenization of metallic precursors, which leads to an accumulation of Ga at the back side of the absorber layer and thus reduces the energy band gap at the absorber surface region.[16] Both technologies discovered that the incorporation of Na as a dopant from the substrate by using soda-lime glass is beneficial.[17,18] A thin chemical-bath-deposited CdS[19,20] or CdZnS[21,22] buffer layer in combination with a mainly sputtered ZnO/ZnO:Al transparent conducting oxide bilayer replaced the previously used evaporated thick indium-doped CdS[11] or CdZnS[23] window layer. The CIGS bilayer process itself was realized by varying the fluxes of the elements so that the layer grows Cu-rich at the beginning and is inverted to a slightly Cu-poor composition at the end of the process, i.e., the preparation of the absorber layer was performed by approaching the photovoltaic active α-phase [near stoichiometric Cu-poor chalcopyrite $Cu(In,Ga)Se_2$] from the Cu-rich side as dictated by the pseudo-binary or -ternary phase diagram.[24–26]

In the next development stage starting in the late 1990s, the bilayer process was gradually replaced by the so-called three-stage process,[27,28] cracking the efficiency mark of 20%[29] for the first time in 2010. The three-stage process is characterized by a Cu-poor/Cu-rich/Cu-poor growth sequence during deposition, initially approaching the photovoltaic relevant α-phase material from the Cu-poor side according to the phase diagram. In parallel, the sequential two-step process was further optimized by the incorporation of sulfur, forming CIGSS to increase the surface band gap due to the Ga accumulation at the back side.[30,31] Both approaches now have a double-graded band gap structure with increased band gap toward the front and back contacts.

In the last 5 years, the solar cell efficiency has again been significantly improved by means of a postdeposition

Contributing Editor: Gary L. Messing
[a]Address all correspondence to this author.
e-mail: dimitrios.hariskos@zsw-bw.de
This paper has been selected as an Invited Feature Paper.
DOI: 10.1557/jmr.2017.394

 © Materials Research Society 2017

https://doi.org/10.1557/jmr.2017.394 Published online by Cambridge University Press

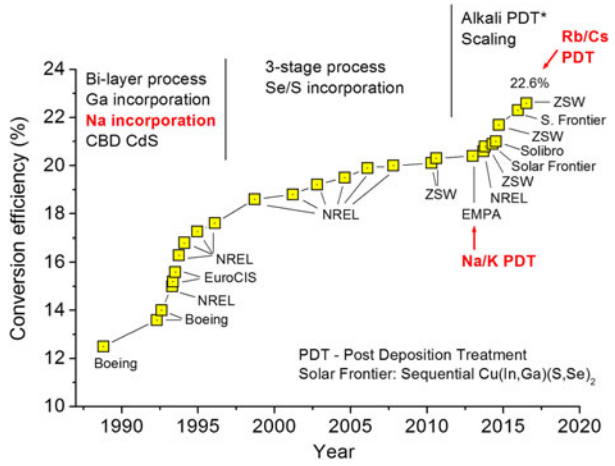


FIG. 1. Efficiency evolution of Cu(In,Ga)Se_2- or Cu(In,Ga)$(S,Se)_2$-based solar cells correlated with different development stages.

treatment (PDT) after the CIGS deposition. The PDT process is now most commonly realized by the evaporation of alkali fluorides in selenium atmosphere on the CIGS surface. The method was first developed in the early 2000s[32] but attracted renewed attention after the realization of a 20.4%-efficient cell on a flexible polyimide substrate at a low CIGS deposition temperature by applying a potassium/sodium PDT.[33] The potassium PDT process was also successfully tested on high-temperature CIGS thin-film layers in different laboratories, promoting the cell efficiency up to 21%.[34,35] In a further development, the heavier alkali metals rubidium Rb and cesium Cs were also implemented, and the highest CIGS cell efficiency could be further improved, first to 21.7%[36] and later to 22.6%.[1] The potassium PDT was proven to also be effective on S-containing sequentially deposited CIGSS layers, leading to certified conversion efficiencies up to 22.3%.[37,38]

In all development stages, Na played an important role for improving the CIGS or CIGSS material properties and thereby increasing the power conversion efficiency of small-area cells and commercial full-size modules. Different methods have been developed for the incorporation of sodium. The various incorporation strategies, detection methods, and the different interpretations of the positive electronic and structural effects of sodium as reported in the literature were summarized and discussed in a recent review article by Salomé et al.[39] The concentration and distribution of sodium in the chalcopyrite absorber layer is influenced by the type of substrate, the Mo back contact, the deposition temperature, and the composition of the absorber layer during the deposition process, i.e., the Cu/(Ga + In) and Ga/(Ga + In) ratios. In addition, a combination of barrier layers and alkali precursor layers can be used for substrate-independent manipulation of the presence of alkali elements during CIGS growth. It has been repeatedly demonstrated that the distribution of Na is not homogeneous; it preferably segregates at grain boundaries and exhibits a much lower concentration inside the grains.[40,41]

The applicability of the heavier alkali homologues for further optimization of the absorber quality was first properly recognized only after implementation of the PDT method. New findings indicate a similar distribution behavior also for the higher homologues K, Rb, and Cs.[42]

In this contribution, we discuss thermodynamic limitations for alkali metals in CIGS and show how they can influence secondary phase formation. We suggest the concept of immiscibility of phases as a tool for interpreting alkali segregation at grain boundaries, formation of clusters in CIGS grains, sporadic formation of microstructures in the CIGS layer (hotspots, nodules), and formation of secondary phases with ordered structures.

II. THERMODYNAMIC ASPECTS

Thermodynamic quantities of chemical reactions related to the CIGS system have been summarized,[43] stability issues discussed,[44–46] and formation energies for point defects calculated from first principle methods.[47–50] In this contribution, we focus on thermodynamic aspects particularly with respect to the interchangeability of Cu and Na in the CIGS system and extend this consideration to the heavier alkali metals K, Rb, and Cs.

To describe the interaction between Cu and Na in Cu(In,Ga)Se_2 or $CuInSe_2$, we refer to the article of Wei et al.,[47] who formulated the following two reactions (1) and (2) and calculated the reaction enthalpy ΔH_R and the mixing enthalpy ΔH_{mix} for them, respectively.

$$\mathrm{Na} + \mathrm{CuInSe_{2(chalcopyrite)}} \leftrightarrows \mathrm{NaInSe_{2(layered)}} + \mathrm{Cu} \quad (1)$$

$$(1-x)\mathrm{CuInSe_2} + x\mathrm{NaInSe_2} \leftrightarrows \mathrm{Na}_x\mathrm{Cu}_{1-x}\mathrm{InSe_2} \quad (2)$$

One can expect the interaction between sodium and $CuInSe_2$ to be much more complicated than that described by the two reactions (1) and (2). Nevertheless, it will turn out that they represent a useful approximation.

Reaction (1) describes the case that atomic Na substitutes for Cu in $CuInSe_2$, forming $NaInSe_2$. The reaction is calculated to be exothermic with a negative reaction enthalpy of $\Delta H_R = -1.9$ eV, i.e., the substitution of Cu by Na is a spontaneous process and can easily take place. On the other hand, for the reverse direction, the enthalpy must be positive ($\Delta H_R = +1.9$ eV) and the reaction will therefore be endothermic, i.e., the replacement of Na by Cu in $NaInSe_2$ is no longer a spontaneous process and will require higher energetic effort. We therefore conclude that it is easier to form $NaInSe_2$ from $CuInSe_2$ than to regenerate $CuInSe_2$ once $NaInSe_2$ has formed.

These findings are in good agreement with experimental observations reported by Rudmann,[51] indicating that

https://doi.org/10.1557/jmr.2017.394 Published online by Cambridge University Press

sodium acts as a barrier for copper diffusion during the second step of the CIGS 3-stage growth process (see Sec. V) at low deposition temperatures below 450 °C. This inhibited diffusion leads to an inhomogeneous Cu distribution in the absorber layer, with excess Cu in the upper and Cu deficiency in the lower part of the layer and disturbed CIGS phase formation which has a detrimental influence on the cell's performance. In contrast, the presence of sodium at higher deposition temperatures in the second stage does not hinder a more homogeneous Cu distribution and enhances absorber properties (although grain sizes are smaller).

An explanation for the experimental observation that the presence of Na decreases copper diffusion at lower temperatures is given by Oikonnen et al.[52] by using density-functional-theory-based calculations. They demonstrated that Na reduces copper mass transport due to the occupation of copper vacancies by Na_{Cu} defects and that this mechanism can also impede V_{Cu}-related cluster formation and lead to measurable effects on defect distribution within the material.

Reaction (2) describes the case that both components, $CuInSe_2$ and $NaInSe_2$, react to form a single-phase compound $Na_xCu_{1-x}InSe_2$. For this chemical conversion, a mixing enthalpy of $\Delta H_{mix} = x\,(1-x)\cdot\Omega$ with $\Omega = 0.67$ eV was calculated.[47] This value is positive for every $x = 0$–1, i.e., the reaction is endothermic for every Na/(Na + Cu) ratio. Endothermic does not mean that reaction (2) is impossible from left to right but that a higher temperature is required for the formation of the quaternary single-phase compound.

To better quantify these findings, it is necessary to consider the Gibbs function of mixing, ΔG_{mix}, which is a measure of the spontaneity of a reaction. For instance, for a generalized reaction $(1-x)A + xB \rightarrow C$, the Gibbs function of mixing $\Delta G_{mix} = \Delta H_{mix} - T\cdot\Delta S_{mix} = G_C - (1-x)G_A - xG_B$, where ΔS_{mix} is the entropy. Since the entropy is always positive,[53] as are T and ΔH_{mix}, the algebraic sign of the Gibbs function will depend on the quantitative relationship between ΔH_{mix} and $T\cdot\Delta S_{mix}$. Higher temperatures will eventually lead to negative ΔG_{mix} values. $\Delta G_{mix} = 0$ describes a reaction in equilibrium; For $\Delta G_{mix} < 0$, the reaction is exergonic, i.e., spontaneous from $A + B \rightarrow C$; and for $\Delta G_{mix} > 0$ the reaction is endergonic, i.e., spontaneous in reverse direction $A + B \leftarrow C$.

Accordingly for reaction (2), the dependence of ΔG_{mix} on the temperature and the calculated ΔH_{mix} can be graphically represented as shown in Fig. 2.

If the temperature is high enough so that $T\cdot\Delta S_{mix} > \Delta H_{mix}$, then $\Delta G_{mix} < 0$ (ΔS_{mix} always positive), and the mixing of $CuInSe_2$ and $NaInSe_2$ to a single-phase compound $Na_xCu_{1-x}InSe_2$ would be a spontaneous process. In contrast, at lower temperatures with $T\Delta S_{mix} < \Delta H_{mix}$, $\Delta G_{mix} > 0$ results and the reverse reaction, i.e., the decomposition to the single compounds $CuInSe_2$ and $NaInSe_2$, would be spontaneous. The lowest required temperature for a single-phase formation is the so-called critical temperature T_C. For ideal binary systems, the influence of the temperature on the curvature of the Gibbs function[54] is described in Fig. 3.

Figure 3 shows the transition from negative ΔG_{mix} values at higher temperatures for an exergonic reaction to positive ΔG_{mix} values at lower temperatures for an endergonic reaction. It is remarkable that for compositions with x close to 0 or to 1, the Gibbs function ΔG_{mix} can assume negative values, even at lower temperatures. This suggests that an extremely small amount of component B can always be dissolved in component A and vice versa.

The translation of the G values from Fig. 3 to a binary phase diagram provides us with the concept of the immiscibility of phases or spinodal decomposition.[55–58] The model can best be illustrated by Fig. 4. It shows the course of the Gibbs function G at two different

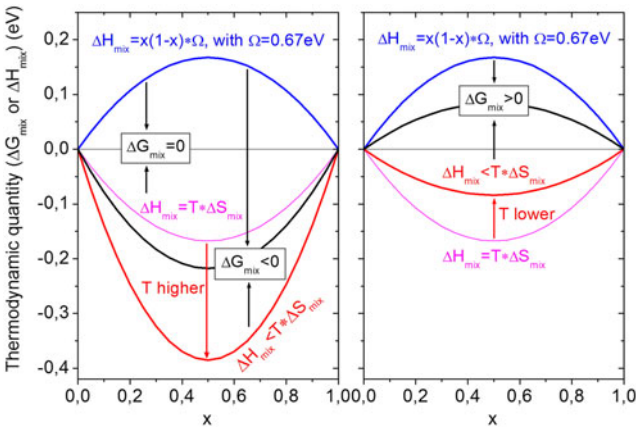


FIG. 2. Gibbs function ΔG_{mix} for reaction (2) in dependence on composition and temperature.

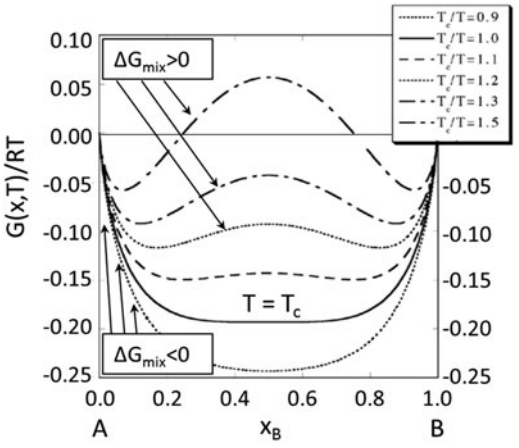


FIG. 3. Curvature of the Gibbs function G for an ideal binary system in dependence on the composition x and the temperature T. T_c is the critical temperature, above which only single phase material exists.

https://doi.org/10.1557/jmr.2017.394 Published online by Cambridge University Press

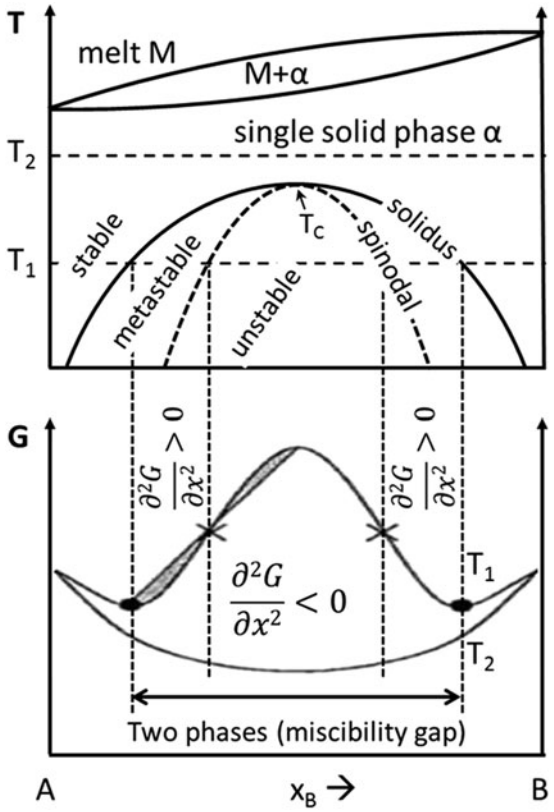


FIG. 4. Concept of spinodal decomposition: Gibbs function and phase diagram with a miscibility gap.

temperatures and the correlation to the phase diagram of an ideal binary system.

At the higher temperature T_2, ΔG_{mix} is negative for every composition x leading to the formation of a stable single phase. At lower temperature T_1, ΔG_{mix} becomes positive for every x between the minima of the G function, leading under equilibrium conditions to the spontaneous decomposition of the material system in two phases (miscibility gap) according to the lever rule as dictated by the binary phase diagram. Outside the miscibility gap, ΔG_{mix} remains negative and allows the existence of a stable single-phase material. The border line is defined by the solidus curve, which corresponds to the minima of the G function with the first derivative $\partial G/\partial x = 0$. The second derivative at the saddle points of the G function $\partial^2 G/\partial x^2 = 0$ defines the spinodal line in the binary phase diagram. Since the second derivative can take positive or negative values within the miscibility gap, this results in a metastable region between the solidus and the spinodal line and in an unstable region under the spinodal line. The two regions are characterized by different decomposition mechanisms (nucleation and growth versus spinodal decomposition) and the separation of different phase morphologies as described in Table I after Chan and Charles.[59]

A positive mixing enthalpy is calculated for reaction (2) between $CuInSe_2$ and $NaInSe_2$. This leads to the situations that, depending on temperature, the Gibbs function ΔG_{mix} can take negative or positive values. The necessary condition where both compounds are stable and can coexist under thermal equilibrium is fulfilled as demonstrated by the calculated stability triangles of the Na–In–Se and the Cu–In–Se system.[47] This allows us to apply the model of spinodal decomposition for the system $CuInSe_2$/$NaInSe_2$. We can expect that under thermal equilibrium, sufficient solubility of $NaInSe_2$ in $CuInSe_2$ to form a quaternary single-phase material would be feasible at low $NaInSe_2$ concentrations and can be increased at higher temperatures (see Fig. 4). For higher $NaInSe_2$ concentrations, we can expect the formation of randomly distributed particles in the metastable region between the spinodal and solidus curve and a two-phase separation in the region under the spinodal curve, according the information in Table I.

TABLE I. Some factors which differentiate between nucleation and growth and spinodal mechanisms during isothermal phase separations (after Chan and Charles[59]) (Reprinted with permission from Ref. 59, Society of Glass Technology, 1965).

Nucleation an growth (metastable region)	Spinodal decomposition (two-phase region)
Invariance of second phase composition to time at constant temperature	Continuous variation of both extremes in composition with time until equilibrium compositions are reached
Interface between phases is always same degree of sharpness during growth	Interface between phases initially is very diffuse, eventually sharpens
Tendency for random distribution of particle sizes and positions in matrix	Regularity of second phase distribution in size and position characterized by a geometric spacing
Tendency for separation of second phase spherical particles with low connectivity	Tendency for separation of second phase, non-spherical particles with high connectivity

III. APPLICABILITY OF THE MODEL FOR FABRICATION OF CIGS THIN FILMS

The model of immiscibility of phases requires equilibrium conditions and stability of the involved compounds. However, the deposition of CIGS or CIGSS thin-film layers is a complicated dynamic nonequilibrium process, which can be carried out by the co-evaporation or the sequential process as described above. The composition of the layer can vary in the Cu/(In + Ga), Ga/(Ga + In), and S/(S + Se) ratio at different locations. CIGS or CIGSS layers are preferentially prepared with element concentration gradients through the layer thickness rather than with a homogeneous element distribution.

The concentration of sodium or other heavier alkali elements (potassium, rubidium, and cesium) in the chalcopyrite absorber layer can be influenced by the

https://doi.org/10.1557/jmr.2017.394 Published online by Cambridge University Press

substrate, the use of alkali-containing precursors, the application of an alkali PDT, deposition temperature profiles, evaporation rates, or partial pressures of the different elements.

Depending on the incorporation methods and the alkali elements used, a variety of binary or ternary alkali metal compounds can theoretically be formed during the chalcopyrite layer processing. Some binary alkali mono or poly selenides (Na_2Se_x,[60] K_2Se_x,[61] Rb_2Se_x,[62] Cs_2Se_x[63]; with $x \geq 1$) and ternary alkali metal seleno indates[64–68] or gallates[67,69,70] which are well known from the literature are summarized in Table II. Most of them have layered structures, i.e., they are rather soft materials and show a limited chemical stability at ambient conditions. For instance, $NaInSe_2$[64] has a layered α-$NaFeO_2$ structure and can be synthesized by the reaction of Na_2Se and In_2Se_3 at 280–300 °C/1.3 × 10^{-4} mbar. The material has a red color and decomposes in humid air (quicker in acidic solutions) to a gray product under the formation of H_2Se or elemental Se.

Under the assumption that some of the alkali compounds from Table II can be formed during the CIGS process and interact locally with the chalcopyrite in quasi-equilibrium with a positive mixing enthalpy ΔH_{mix}, even for a while, we can expect scenarios as schematically indicated in Fig. 5 for our system. Since the incorporation of alkali elements in CIGS only aims at doping-level concentrations, only the left side of the binary phase diagram is of interest, i.e., for x_B values close to zero. As mentioned above, according to the calculated stability triangles of the Na–In–Se and the Cu–In–Se system,[47] the only Na compound that can coexist under thermal equilibrium with $CuInSe_2$ is $NaInSe_2$. The binary $NaSe_2$ is excluded. Therefore, for Fig. 5, only the ternary alkali compounds were considered as the possible component B. The alkali elements can diffuse into the CIGS layer from the glass substrate at elevated temperatures or can be provided in Se atmosphere from a precursor layer or by PDT as an alkali fluoride. Selenium is needed for the removal of fluoride as gaseous selenium fluoride during the PDT process. The alkali receptivity of the CIGS layer will be limited by the solidus curve and the deposition temperature. On exceeding the solidus or spinodal curve toward a higher alkali concentration, x_B, during the alkali supply or toward a lower temperature during cooling down, alkali-rich secondary phase separation will result according to the lever rule as dictated by the phase diagram. As shown in Table I, depending on the alkali concentration and the temperature, the separation of the secondary phases will be influenced by different mechanisms (metastable or two-phase region). However, to be able to make qualitative or quantitative assessments for the CIGS deposition process according to the model, it is important to have the information about the alkali compounds which are actually formed in CIGS as determined by the kinetics and to know the Gibbs function $G(x,T)$ of the defined equilibria.

In the following, we refer to examples from the literature for inhomogeneous alkali distribution, segregations at grain boundaries, formation of clusters or microstructures, and the separation of secondary phases with ordered structures as observed in CIGS layers, and correlate them with the model as schematically represented by Fig. 5. We will focus on the coevaporation technology.

Of course, the distribution of alkali metals in CIGS cannot be only interpreted as a result of phase separation according to the model but also as a consequence of diffusion processes from the substrate[71,72] during the CIGS layer growth or after a PDT,[73] in particular for the extremely low alkali concentrations desired for CIGS doping. Other models that could explain these phenomena as well as the influence of kinetic aspects are not discussed in this article.

TABLE II. Some known alkali metal selenides and alkali seleno indates or gallates.

Binary and ternary alkali compounds	
Mono selenides:	Na_2Se, K_2Se, Rb_2Se, Cs_2Se
Poly selenides:	Na_2Se_x, K_2Se_x, Rb_2Se_x, Cs_2Se_x with $x > 1$
Seleno indates:	$NaInSe_2$, $Na_7In_3Se_s$, $Na_21n_6Se_{10}$ $KInSe_2$ $RbinSe_2$, $Rbin_7Se_9$, $Rb_4In_2Se_5$ $CsIn_7Se_9$
Seleno gallates:	$NaGaSe_2$, $NaGa_3Se_5$, $Na_2Ga_2Se_3$, $Na_6Ga_2Se_6$ K_5GaSe_4, $K_6Ga_2Se_6$ $RbGaSe_2$ $CsGaSe_3$, $Cs_6Ga_2Se_3$, $Cs_8Ga_4Se_{10}$, $Cs_{10}Ga_6Se_{14}$

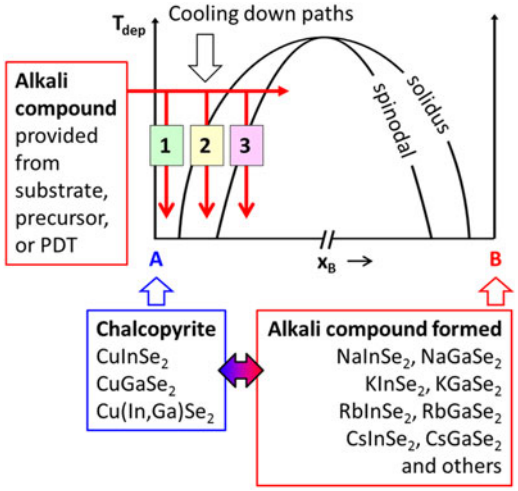


FIG. 5. Schematic representation for interaction scenarios between chalcopyrite and alkali compounds during Cu(In,Ga)Se_2 processing. Cooling down paths: [1] single phase formation, [2] formation of randomly distribution of particles, and [3] secondary phase separation.

https://doi.org/10.1557/jmr.2017.394 Published online by Cambridge University Press

IV. EXAMPLES FOR ALKALI SEGREGATIONS IN CIGS FROM THE LITERATURE

Atom Probe Tomography (APT) measurements have shown that the distribution of sodium in the bulk of polycrystalline thin-film CIGS layers is not homogeneous. The concentration inside the grains is much lower than that on the grain boundaries. Inside the grains, sodium atoms were found to be distributed homogeneously with concentrations in the range of 20 ppm (0.002 at.%) for $CuInSe_2$[40] and 85 ppm (0.0085 at.%) for $Cu(In,Ga)Se_2$.[41] However, it is not statistically validated that the solubility of sodium in $Cu(In,Ga)Se_2$ is principally higher than that in $CuInSe_2$ grains. In contrast, sodium concentrations up to 50 at.% were detected on grain boundaries.[74] The measured concentrations in the grains may correspond to the solubility limit of sodium in the chalcopyrite after cooling down from the high-process temperature (~600 °C) to a lower temperature (Fig. 5, cooling down path 1). According to the model, the accumulation of sodium at the grain boundaries may be interpreted as the first indication for the beginning of a phase separation in the metastable region very close to the solidus curve (Fig. 5, cooling down path 2).

The formation of randomly distributed particles with low connectivity in the metastable region or separation of the regular secondary phase with high connectivity in the two-phase region (see Table I) can be expected for higher sodium concentrations. We can find many examples in the literature which can be correlated to a phase separation in the miscibility gap of the metastable as well as the unstable region.

In a comparative study, as reported by Choi et al.[75] CIGS was deposited by a single-stage co-evaporation process on glass and steel substrates, both with an NaF precursor layer on the Mo back contact, and the distribution of Na in CIGS was analyzed by APT and other methods. The Na dopant concentration was varied until the CIGS layer contained a significant amount of Na impurities. It was found that Na is inhomogeneously distributed and is segregated at GB's and clusters inside the grains. At grain boundaries, sodium partly occupies Cu vacancies, compensating the formation of In_{Cu} point defects and thus contributing to the enhanced cell efficiency. The formation of clusters is explained by the limited solubility of Na in CIGS and can be interpreted according the model as a "phase" separation in the metastable region close to the solidus curve. The average Na concentration in the clusters is found to be 14.0 ± 0.5 at.%. Figure 6(a) shows a three-dimensional $118 \times 112 \times 487$ nm^3 sodium elemental map in the absorber film of the sample on glass as determined by APT. Several Na-rich clusters are resolved as marked by the arrows.

Contreras et al.[76] reported on the characterization of CIGS polycrystalline thin films on substrates which were coated with thin precursor layers (~200 Å) of NaF, KF, and CsF prior to ClGS deposition and their growth by coevaporation from elemental sources. The precursor layers provided an impurity molar concentration of ~3% with respect to the ~2 μm thick ClGS layers. In samples grown with excessive Na (>400 Å NaF in the precursor film), formation of secondary phases were observed. In CIGS absorbers with Ga/(Ga + In) ~0.3, such secondary phases were characterized by three strong diffraction lines at 2θ ~12.4, ~24.8, and ~37.6. Similar secondary phases were also detected in $CuInSe_2$ and $CuGaSe_2$. All these secondary phases were not identified but assumed to be a form of $Cu_uNa_y(In,Ga)_wSe_z$ compounds. A comparison of the X-ray diffraction (XRD) peaks of the unknown secondary phase formed in $CuInSe_2$ with the database of the International Center for Diffraction Data (ICDD or JCPDS)[77] shows that the unknown phase corresponds to the peaks of $NaInSe_2$ that was synthesized and characterized by Hoppe et al.[64]

Lin et al.[78] reported on the deposition of CIGS thin films on Mo/SiO_x/stainless steel substrates by magnetron sputtering. The Na was supplied to the CIGS layer through a Mo:Na/Mo back contact layer that was sputtered from a metallic Mo–5%Na target. It was found that excess of the Na dopant in CIGS arising from an Na content in the Mo layer above 2.8% does not contribute to the phase crystallization of CIGS and leads to the formation of the $NaInSe_2$ secondary phase. The formation of secondary phases increases the number of In vacancies and reduces the grain size of the chalcopyrite layer, compromising crystallinity.

Lee et al.[79] reported on the formation of nodules in CIGS layers prepared by a roll-to-roll three-stage coevaporation process. The CIGS layers were grown with a Ga/(In + Ga) ratio of ~0.37 on Mo-coated stainless steel substrates. Na was provided to the CIGS material by an NaF precursor evaporated onto the Mo-coated stainless steel substrate prior to CIGS deposition. The final Cu-poor CIGS composition was realized via an intermediate phase transformation to Cu-rich CIGS from a $(In,Ga)_2Se_3$ composition in the first stage of the process. It was observed that nodule formation was induced by a higher temperature in the first stage of the evaporation process. By controlling the growth of the $(In,Ga)_2Se_3$ film at low substrate temperatures, nodule formation could be eliminated, and the open circuit voltage V_{OC} and the efficiency of cells significantly improved. The nodules were found to have a reduced Cu content and a sodium concentration higher than 0.2 at.% (>2000 ppm) as measured by energy-dispersive X-ray spectroscopy (EDS). A size distribution of 2–4 μm was found by high-resolution electroluminescence imaging [Fig. 6(b)]. Without the NaF precursor, no sign of nodule formation was observed even at a higher temperature in the first step. The effect of nodule formation

https://doi.org/10.1557/jmr.2017.394 Published online by Cambridge University Press

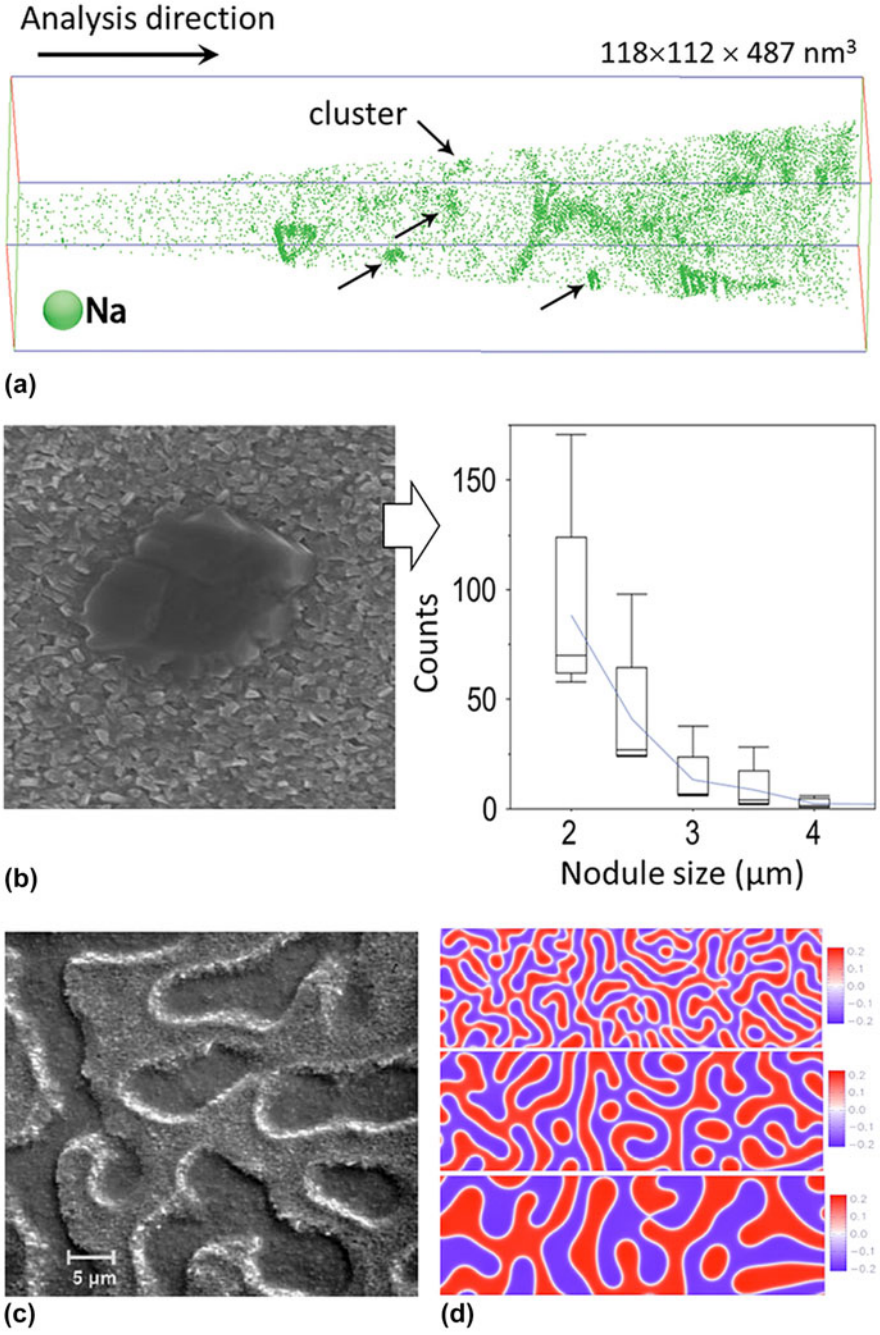


FIG. 6. Examples of secondary phase separation: (a) Formation of Na-rich clusters in the grains of Cu(In,Ga)Se_2 layers containing a significant amount of sodium, as detected by atom probe tomography by Choi et al.,[75] (b) formation and size distribution of nodules in Cu(In,Ga)Se_2 layers prepared on stainless steel substrate with NaF precursor at high substrate temperatures in the 1st stage of the three-stage process (according to Lee et al.[79]), (c) scanning electron micrograph of a Ga-rich $CuGaSe_2$ thin film on the Na-containing Mo-coated glass substrate showing secondary phase structures with reduced Cu and increased Na content (according to Nadenau et al.[80]), and (d) example of phase separation during spinodal decomposition according to the Cahn-Hilliard model[54] (Adapted with permission from Ref. 75, AIP Publishing LLC, 2011; Ref. 79, IEEE, 2016; Ref. 80, Elsevier, 2001; Ref. 54, John Wiley and Sons, 2010).

in the CIGS layer can be correlated to the model since increased sodium diffusion in the $(In,Ga)_2Se_3$ layer will form thermodynamically stable Na–In/Ga–Se compounds, which cannot be dissolved in the chalcopyrite phase or will separate after cooling down in the metastable region of the binary phase diagram (compare Fig. 5 and Sec. V).

Nadenau et al.[80] reported on sodium-induced secondary phase segregation in $CuGaSe_2$ layers which were grown by simultaneous multi-source evaporation of the

https://doi.org/10.1557/jmr.2017.394 Published online by Cambridge University Press

elements on soda-lime glass at substrate temperatures of approximately 600 °C. The segregations were regularly structured with typical dimensions in the order of 5 μm and covering more than half of the film area. The secondary structures were characterized by a reduced thickness and an increased Ga/(Ga + Cu) ratio of approximately 0.75, correspondingly a reduced copper concentration, as well as an increased sodium content by a factor of seven compared to the surrounding material. The density of secondary structures increased with increasing the Ga content, i.e., with a reduced Cu content. A scanning electron microscopy (SEM) micrograph of a Ga-rich $CuGaSe_2$ thin film including a high density of secondary phase structures is shown in Fig. 6(c). Micro-Raman spectroscopy analysis revealed a nonchalcopyrite phase with a structure very similar to that of $CuGa_3Se_5$. The authors suggested the formation of a quaternary Na–Cu–Ga–Se compound with the defect-chalcopyrite structure $CuGa_3Se_5$, but with the Cu-vacancies partially filled by Na atoms. According to the information in Table I, the effect of separation of regular secondary Cu-poor/Na-rich phases in $CuGaSe_2$ can be correlated to a phase separation in the unstable region of the miscibility gap (Fig. 5). The regularity and connectivity of the secondary phase structures resemble the phase separation during spinodal decomposition according to the Cahn–Hilliard model[54] [Fig. 6(d)].

Similar Na-rich aggregates were reported by Balboul et al.,[81] also for the case of $CuInSe_2$ polycrystalline thin-films but only in early stages of film formation. By varying the Se activity during the absorber deposition, it was found that the formation of sodium-induced secondary phases is inhibited at high Se rates.

Segregation of Cu-poor/Na-rich species in CIGS is a phenomenon that was also observed at the surface of thin-film layers contained a higher Na concentration. Song et al.[82] studied the impact of Na on the chemical and electronic surface structure of CIGS absorbers with various Cu-contents deposited at comparatively low temperatures in the range of 420 °C by using X-ray photoelectron and X-ray excited Auger electron spectroscopy. Sodium was incorporated into the CIGS chalcopyrite thin-film absorbers deposited on Mo-coated polyimide flexible substrates by adding differently thick layers of NaF in-between the CIGS absorber and Mo back contact. It was found that the CIGS surface composition of all samples independently on the bulk composition (Cu rich or Cu poor) or the content of segregated Na from bulk to the surface is in accordance with the Cu-depleted 1:3:5 composition as earlier reported.[83–85] However, besides this general behavior, for the highest Na contents, authors found clear indications for the formation of a (Cu,Na)–(In,Ga)–Se-like surface compound, such as $Cu_2Na_3(In,Ga)_5Se_{10}$.

Heavier alkali metal dopants (K, Rb, and Cs) are most typically deposited on the surface of the CIGS layer by a PDT and can be incorporated into the CIGS layer depending on the substrate temperature. Similar to the alkali supply from the substrate, secondary phase segregation can also be induced by the heavier alkali element after the PDT. The prerequisite for this is that the provided amount exceeds the solubility limits as dictated by the solidus curve. The formation of the secondary phase on the CIGS surface after a NaF/KF PDT was reported by Reinhard et al.[86] A composition analysis was performed by inductively coupled plasma mass spectrometry (ICP-MS) after dissolving the surface material in H_2O or diluted HCl. It was found to consist of the elements Na/K/In/Ga/Se with an insignificant amount of Cu (Fig. 7).

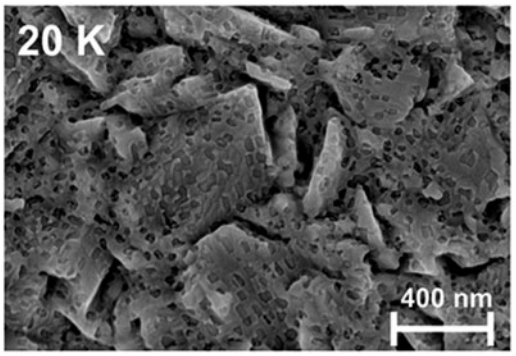


FIG. 7. Formation of microstructures on the $Cu(In,Ga)Se_2$ surface after a Na/K post deposition treatment with a Na/K/In/Ga/Se composition according to Reinhard et al.[86] (Reproduced with permission from Ref. 86, ACS Publications, 2015).

The influence of the NaF/KF PDT on the chemical surface structure of $Cu(In,Ga)Se_2$ was also investigated by Handick et al.[87] by using synchrotron-based hard X-ray photoelectron spectroscopy (HAXPES) and SEM. With increasing amounts of alkali fluorides, the surface structure was found to contain more potassium combined with a higher degree of Cu and Ga depletion, indicating the formation of a K–In–Se-type surface layer.

The distribution of heavier alkali metals in CIGS is the subject of very recent investigations. First results with APT[42] show that the solubility in CIGS grains strongly decreases with the increasing size of the alkali element and drops below the detection limit. Heavier alkali metals accumulate at grain boundaries and displace the lighter alkali element Na.

The solubility limit of all alkali elements (Li, Na, K, Rb, and Cs) in $CuInSe_2$ was determined by first principle calculations depending on the temperature by Malitckaya et al.,[88] and mechanisms for the secondary phase formation following the PDT process were suggested. Based on the calculated reaction enthalpies and migration considerations, they found that mixed phases are more likely in the case of $LiInSe_2$ and $NaInSe_2$, while formation of segregated phases are expected for $KInSe_2$, $RbInSe_2$, and $CsInSe_2$.

https://doi.org/10.1557/jmr.2017.394 Published online by Cambridge University Press

V. CORRELATION OF THE CIGS 3-STAGE PROCESS WITH THE ALKALI METAL SUPPLY

The three-stage process was empirically developed with the aim to approach the photovoltaic active α-phase initially from the Cu-poor side of the phase diagram. Typical profiles for temperatures and relative evaporation rates of Cu, In, and Ga during the CIGS three-stage process are demonstrated in Fig. 8.

In the 1st stage, a Cu-free or Cu-poor $(In,Ga)_xSe_y$ layer is deposited at relatively low substrate temperatures of 400–450 °C. In the 2nd stage, the evaporation rate of Cu is increased, whereas the In and Ga rates are reduced. The incorporation of Cu is performed at elevated process temperatures up to 600–700 °C and leads to the transformation of the Cu-poor precursor to Cu-rich Cu(In,Ga)Se_2. In the 3rd stage, the desired final Cu-poor CIGS composition is realized by reducing the evaporation rate of Cu and simultaneously increasing the evaporation rates of In and Ga. The process ends after cooling down to room temperature.

But how can we interpret the necessity of a lower temperature at the 1st and a higher one at the 2nd stage and the influence of an abrupt or a slow cooling down phase on the chalcopyrite layer properties, and how does this correlate with the sodium content in the chalcopyrite layer?

Couzinie-Devy et al.[89] analyzed the sodium concentration in CIGS at key points of the 3-stage process by atom probe tomography. 3D atom distributions were reconstructed for three samples namely A, B, and C which originated from the 1st stage (T = 400 °C, Cu poor), the 2nd stage (T = 630 °C, Cu rich), and the 3rd stage (T = 630 °C, completed CIGS layer, slightly Cu poor), respectively. Different sodium concentrations inside the grains were detected for the different stages of the evaporation process: for sample A ~300 at. ppm, for sample B <10 at. ppm (below the detection limit), and for sample C ~50 at. ppm. These findings show that the sodium concentration in CIGS during processing is not constantly at the same level but fluctuates depending on the temperature and the composition of the layer. The highest sodium concentration in the layer was detected during the first stage (when the material composition is Cu poor) although the temperature is lowest.

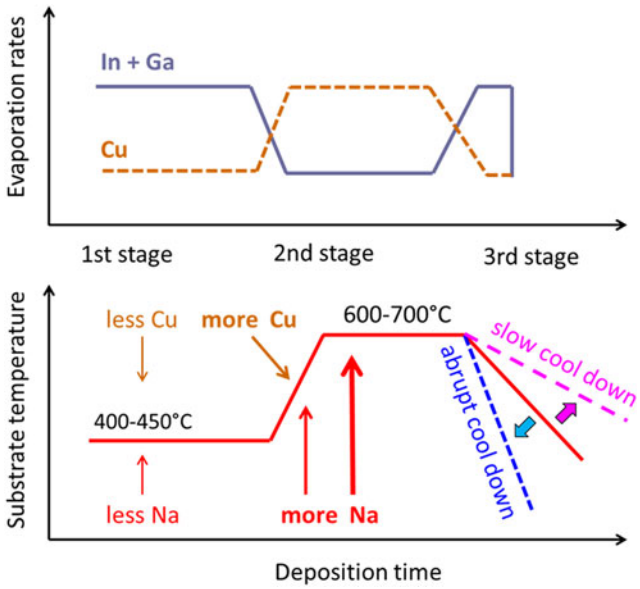


FIG. 8. Evaporation rates for Cu versus In/Ga and substrate temperature profiles during the Cu(In,Ga)Se_2 three-stage process.

In the 1st stage, a higher temperature would stimulate enhanced sodium diffusion from the glass substrate[90] into the Cu-poor $(In,Ga)_2Se_3$ layer, easily forming stable Na(In,Ga)Se_2 phases. Considering the thermodynamic limitations for the exchangeability of Na by Cu according reaction (1), we can expect that the dissolution of these alkali phases would be difficult and will require an increased energetic effort. A low temperature in the first step is therefore beneficial.

In the second stage, the increased temperature facilitates higher sodium diffusion from the substrate. However, the formation of secondary Na-rich phases like seleno indates or gallates is compensated by the simultaneous Cu diffusion. The mid–stage transition of CIGS to a Cu-rich composition further reduces the material's capacity for sodium incorporation. The high temperature in the second stage thus supports the reduction of the sodium concentration in CIGS by evaporation and is also advantageous for the dissolution of the remaining secondary sodium-rich phases. Sodium evaporation from the CIGS layer during deposition is experimentally confirmed. Colombara et al.[91] reported on sodium transport by evaporation from the CIGS layer matrix into the deposition system, which caused incidental gas-phase alkali doping on other chalcopyrite layers prepared on sodium-free substrates.

In the 3rd stage, the cooling down temperature gradient will determine the grain size and the sodium concentration ratio between grains and grain boundaries. An abrupt cooling down will lead to the formation of smaller grains, which, however, contain a higher amount of Na and a reduced sodium segregation at grain boundaries (quenching effect, kinetical limitation). In contrast, a slower cooling down will lead to the formation of larger grains containing lower amounts of sodium, accompanied with an increased accumulation of sodium at grain boundaries (thermodynamic limitation). Influencing the amount of sodium in the grains or in the grain boundaries provides an extra leverage for further influencing the electrical properties of CIGS layers.[92]

VI. CONCLUSION

Consequences of the positive mixing enthalpy of the $CuInSe_2/NaInSe_2$ system on the processing of CIGS thin

https://doi.org/10.1557/jmr.2017.394 Published online by Cambridge University Press

films were presented. The concept of immiscibility of phases (spinodal decomposition) was suggested as a tool for the interpretation of secondary phase formation. However, additional work is needed to determine realistic dynamic equilibria and associated thermodynamic quantities. Examples from the literature were presented indicating that higher amounts of alkali dopants in CIGS induce the formation of secondary phases as particles or regular phases with an alkali-rich and Cu-poor composition. The 3-stage process was analyzed with respect to the sodium content in CIGS during the layer growth.

ACKNOWLEDGMENTS

This work was financially supported by the German Federal Ministry of Economic Affairs and Energy (BMWi) within different projects. Authors would like to thank the ZSW team for valuable literature references and discussions, Rommel Noufi for constructive discussions, and Theresa Magorian-Friedlmeier for reviewing the manuscript.

REFERENCES

1. P. Jackson, R. Wuerz, D. Hariskos, E. Lotter, W. Witte, and M. Powalla: Effects of heavy alkali elements in Cu(In,Ga)Se_2 solar cells with efficiencies up to 22.6%. *Phys. Status Solidi RRL* **10**, 583–586 (2016).
2. Solar Frontier: Press release (2017). Available at: http://www.solar-frontier.com/eng/news/2017/0227_press.html (accessed February 27, 2017).
3. Solibro: Press release (2017). Available at: http://solibro-solar.com/en/news-downloads/news/ (accessed January, 2017).
4. U.P. Singh and S.P. Patra: Progress in polycrystalline thin-film Cu(In,Ga)Se_2 solar cells. *Int. J. Photoenergy*, **2010**, Article ID 468147 (2010). doi: 10.1155/2010/468147.
5. D. Abou-Ras, S. Wagner, B.J. Stanbery, H-W. Schock, R. Scheer, L. Stolt, S. Siebentritt, D. Lincot, C. Eberspacher, K. Kushiya, and A.N. Tiwari: Innovation highway: Breakthrough milestones and key developments in chalcopyrite photovoltaics from a retrospective viewpoint. *Thin Solid Films* **633**, 2–12 (2017).
6. S. Niki, M. Contreras, I. Repins, M. Powalla, K. Kushiya, S. Ishizuka, and K. Matsubara: CIGS absorbers and processes. *Prog. Photovoltaics* **18**, 453–466 (2010).
7. W.N. Shafarman, S. Siebentritt, and L. Stolt: Cu(InGa)Se_2 Solar Cells. In *Handbook of Photovoltaic Science and Engineering*, 2nd ed., A. Luque and S. Hegedus, eds. (John Wiley & Sons, Chippenham, Wiltshire, U.K., 2011); pp. 546–599.
8. S.R. Kodigala, ed.: Cu($In_{1-x}Ga_x$)Se_2 and CuIn($Se_{1-x}S_x$)$_2$ thin film solar cells. In *Thin Films and Nanostructures (Book Series)*, Vol. **35** (Academic Press, U.K., 2010); pp. 2–685.
9. R. Scheeer and H.W. Schock: *Chalcogenide Photovoltaics*, 1st ed. (WILEY-VCH Verlag & Co. KGaA, Singapore, 2011).
10. National Renewable Energy Laboratory NREL. Available at: https://www.nrel.gov/pv/assets/images/efficiency-chart.png (accessed September 12, 2017).
11. R.A. Mickelsen and W.S. Chen: Development of a 9.4% efficient thin-film $CuInSe_2$/CdS solar cell. In *Rec. 15th IEEE Photovoltaic Spec. Conf., Kissimmee, Florida, May 12–15* (IEEE, New York, 1981); pp. 800–804.
12. R. Klenk, T. Walter, H-W. Schock, and D. Cahen: A model for the successful growth of polycrystalline films of $CuInSe_2$ by multisource physical vacuum evaporation. *Adv. Mater.* **5**, 114–119 (1993).
13. W.S. Chen, J.M. Stewart, B.J. Stanbery, W.E. Devaney, and R.A. Mickelsen: Development of thin film polycrystalline $CuIn_{1-x}Ga_xSe_2$ solar cells. In *Rec. 19th IEEE Photovoltaic Spec. Conf., New Orleans, Louisiana, May 4–8* (IEEE, New York, 1987); pp. 1445–1447.
14. V.K. Kapur, U.V. Choudary, and A.K.P. Chu: Process of forming a compound semiconductive material. US Patent No. 4,581,108, 1986.
15. K. Mitchell, C. Eberspacher, J. Ermer, and D. Pier: Single and tandem junction $CuInSe_2$ cell and module technology. In *Rec. 20th IEEE Photovoltaic Spec. Conf., Las Vegas, Nevada, September 26–30* (IEEE, New York, 1988); pp. 1384–1389.
16. C.L. Jensen, D.E. Tarrant, J.H. Ermer, and G.A. Pollock: The role of Gallium in $CuInSe_2$ solar cells fabricated by a two stage method. In *Rec. 23rd IEEE Photovoltaic Spec. Conf., Louisville, Kentucky, May 10-14* (IEEE, New York, 1993); pp. 577–580.
17. K.W. Mitchell, C. Eberspacher, J.H. Ermer, K.L. Pauls, and D.N. Pier: $CuInSe_2$ cells and modules. *IEEE Trans. Electron Devices* **37**, 410–417 (1990).
18. J. Hedström, H. Ohlsén, M. Bodegård, A. Kylner, L. Stolt, D. Hariskos, M. Ruckh, and H.W. Schock: ZnO/CdS/Cu(In,Ga)Se_2 Thin film solar cells with improved performance. In *Rec. 23rd IEEE Photovoltaic Spec. Conf., Louisville Kentucky, May 10–14* (IEEE, New York, 1993); pp. 364–371.
19. R.R. Potter: Enhanced photocurrent ZnO/CdS/$CuInSe_2$ solar cells. *Sol. Cells* **16**, 521–527 (1986).
20. J. Kessler, K.O. Velthaus, M. Ruckh, R. Laichinger, H.W. Schock, D. Lincot, R. Ortega, and J. Vedel: Chemical bath deposition of CdS on $CuInSe_2$, etching effects and growth kinetics. In *Proc. 6th Int. Photovoltaic Sci. Eng. Conf. (PVSEC-6), New Delhi, India, February 10–14*, B.K. Das and S.N. Singh, eds. (Oxford & Ibh Publishing Co. Pvt. Ltd., New Delhi, 1992); pp. 1005–1010.
21. W.E. Deveney, W.S. Chen, J.M. Stewart, and R.B. Gilette: High efficiency $CuInSe_2$ and $CuInGaSe_2$ based cells and materials research. In *Final Technical Progress Report for the Contract ZL-8-06031-8, Period 1987–1989* (Boing Electronics High Technology Center, Seattle, Washington, 1990); pp. 17–19.
22. R.K. Ahrenkiel, L.L. Kazmerski, R.J. Matson, C. Osterwald, T.P. Massopust, R.A. Mickelsen, and W.S. Chen: Heterojunction formation in (CdZn)S/$CuInSe_2$ ternary solar cells. *Appl. Phys. Lett.* **43**, 658–660 (1983).
23. R.A. Mickelsen and W. Chen: Polycrystalline thin-film $CuInS_2$ solar cells. In *Rec. 16th IEEE Photovoltaic Spec. Conf., San Diego, California, September 27–30* (IEEE, New York, 1982); pp. 781–785.
24. T. Goedecke, T. Haalboom, and F. Ernst: Phase equilibria of Cu–In–Se. I. Stable states and nonequilibrium states of the In_2Se_3–Cu_2Se subsystem. *Z. Metallkd.* **91**, 622–634 (2000).
25. C. Beilharz: Charakterisierung von aus der Schmelze gezüchteten Kristallen in den Systemen Kupfer–Indium–Selen und Kupfer–Indium–Gallium–Selen für photovoltaische Anwendungen. Ph.D. dissertation, Shaker Verlag, Aachen, 1999.
26. B.J. Stanbery: Copper indium selenides and related materials for photovoltaic devices. *Crit. Rev. Solid State Mater. Sci.* **27**, 73–117 (2002).
27. M.A. Contreras, J.R. Tuttle, A. Gabor, A. Tennant, K. Ramanathan, S. Asher, A. Franz, J. Keane, L. Wang, J. Scofield, and R. Noufi: High efficiency Cu(In,Ga)Se_2-based solar cells: Processing of novel absorber structures. In *Rec. 24th IEEE Photovoltaics Spec. Conf. (1st WCPEC), Waikoloa, Hawaii, December 5–9* (IEEE, New York, 1994); pp. 68–75.

https://doi.org/10.1557/jmr.2017.394 Published online by Cambridge University Press

28. I. Repins, M.A. Contreras, B. Egaas, C. DeHart, J. Scharf, C.L. Perkins, B. To, and R. Noufi: 19.9%-efficient ZnO/CdS/CuInGaSe_2 solar cell with 81.2% fill factor. *Prog. Photovoltaics* **16**, 235–239 (2008).
29. P. Jackson, D. Hariskos, E. Lotter, S. Paetel, R. Wuerz, R. Menner, W. Wischmann, and M. Powalla: New world record efficiency for Cu(In,Ga)Se_2 thin-film solar cells beyond 20%. *Prog. Photovoltaics* **19**, 894–897 (2011).
30. Y. Tanaka, N. Akema, T. Morishita, D. Okumura, and K. Kushiya: Improvement of V_{OC} upward of 600 mV/cell with CIGS-based absorber prepared by selenization/sulfurization. In *Proc. 17th Eur. Photovoltaic Sol. Energy Conf., Munich, Germany, October 22–26*, B. McNelis, W. Palz, H.A. Ossenbrink, and P. Helm, eds. (WIP, Munich, Germany, 2001); pp. 989–994.
31. J. Palm, V. Probst, and F.H. Karg: Second generation CIS solar modules. *Sol. Energy* **77**, 757–765 (2004).
32. O.D. Rudmann and A.N. Tiwari: Verfahren zur Herstellung einer Verbindungshalbleiterschicht mit Alkalizusatz, Patent DE 102 59 258 B4 2006.03.16, December 11, 2002.
33. A. Chirilă, P. Reinhard, F. Pianezzi, P. Bloesch, A.R. Uhl, C. Fella, L. Kranz, D. Keller, C. Gretener, H. Hagendorfer, D. Jaeger, R. Erni, S. Nishiwaki, S. Buecheler, and A.N. Tiwari: Potassium-induced surface modification of Cu(In,Ga)Se_2 thin films for high-efficiency solar cells. *Nat. Mater.* **12**, 1107–1111 (2013).
34. P. Jackson, D. Hariskos, R. Wuerz, W. Wischmann, and M. Powalla: Compositional investigation of potassium doped Cu(In,Ga)Se_2 solar cells with efficiencies up to 20.8%. *Phys. Status Solidi RRL* **8**, 219–222 (2014).
35. O. Lundberg, E. Wallin, V. Gusak, S. Södergren, S. Chen, S. Lotfi, F. Chalvet, U. Malm, N. Kaihovirta, P. Mende, G. Jaschke, P. Kratzert, J. Joel, M. Skupinski, P. Lindberg, T. Jarmar, J. Lundberg, J. Mathiasson, and L. Stolt: Improved CIGS modules by KF post deposition treatment and reduced cell-to-module losses. In *Rec. 43rd IEEE Photovoltaic Spec. Conf., Portland, Oregon, June 5–10* (IEEE, New York, 2016); pp. 1293–1296.
36. P. Jackson, D. Hariskos, R. Wuerz, O. Kiowski, A. Bauer, T.M. Friedlmeier, and M. Powalla: Properties of Cu(In,Ga)Se_2 solar cells with new record efficiencies up to 21.7%. *Phys. Status Solidi RRL* **9**, 28–31 (2015).
37. R. Kamada, T. Yagioka, S. Adachi, A. Handa, K.F. Tai, T. Kato, and H. Sugimoto: New world record Cu(In,Ga)$(Se,S)_2$ thin film solar cell efficiency beyond 22%. In *Rec. 43rd IEEE Photovoltaic Spec. Conf.* (2016); pp. 1287–1291.
38. T. Kato: Cu(In,Ga)$(Se,S)_2$ solar cell research in solar Frontier: Progress and current status. *Jpn. J. Appl. Phys.* **56**, 04CA02 (2017).
39. P.M.P. Salomé, H. Rodriguez-Alvarez, and S. Sadewasser: Incorporation of alkali metals in chalcogenide solar cells. *Sol. Energy Mater. Sol. Cells* **143**, 9–20 (2015).
40. O. Cojocaru-Mirédin, P. Choi, R. Wuerz, and D. Raabe: Atomic-scale distribution of impurities in $CuInSe_2$-based thin-film solar cells. *Ultramicroscopy* **111**, 552–556 (2011).
41. E. Cadel, N. Barreau, J. Kessler, and P. Pareige: Atom probe study of sodium distribution in polycrystalline Cu(In,Ga)Se_2 thin film. *Acta Mater.* **58**, 2634–2637 (2010).
42. A. Vilalta-Clemente, C. Castro, M. Raghuwanshi, S. Duguay, E. Cadel, P. Pareige, P. Jackson, D. Hariskos, R. Wuerz, and W. Witte: Distribution of alkali elements in Cu(In,Ga)Se_2 solar cells on a nanometer scale. Presented at the *Symp. E, Eur. Mater. Res. Soc. Meet. (EMRS), Strasburg, France, May 22–26, 2017 (EMRS, 2017), Symp. E, No E.III.3*. (2017).
43. D. Cahen and R. Noufi: Free energies and enthalpies of possible gas phase and surface reactions for preparation of $CuInSe_2$. *J. Phys. Chem. Solids* **53**, 991–1005 (1992).
44. J-F. Guillemoles, L. Kronik, D. Cahen, U. Rau, A. Jasenek, and H. Werner Schock: Stability issues of Cu(In,Ga)Se_2-based solar cells. *J. Phys. Chem. B* **104**, 4849–4862 (2000).
45. J.F. Guillemoles: Stability of Cu(In,Ga)Se_2 solar cells: A thermodynamic approach. *Thin Solid Films* **361–362**, 338–345 (2000).
46. J.F. Guillemoles: The puzzle of Cu(In,Ga)Se_2 (CIGS) solar cells stability. *Thin Solid Films* **403–404**, 405–409 (2002).
47. S-H. Wei, S.B. Zhang, and A. Zunger: Effects of Na on the electrical and structural properties of $CuInSe_2$. *J. Appl. Phys.* **85**, 7214–7218 (1999).
48. J. Pohl and K. Albe: Thermodynamics and kinetics of the copper vacancy in $CuInSe_2$, $CuGaSe_2$, $CuInS_2$, and $CuGaS_2$ from screened-exchange hybrid density functional theory. *J. Appl. Phys.* **108**, 023509 (2010); *J. Appl. Phys.* **110**, 109905 (2011).
49. C. Persson, Y-J. Zhao, S. Lany, and A. Zunger: n-Type doping of $CuInSe_2$ and $CuGaSe_2$. *Phys. Rev. B* **72**, 035211 (2005).
50. M. Malitckaya, H-P. Komsa, V. Havu, and M.J. Puska: First-principles modeling of point defects and complexes in thin-film solar-cell absorber $CuInSe_2$. *Adv. Electron. Mater.* **3**, 1600353 (2017).
51. D. Rudmann: Effects of sodium on growth and properties of Cu(In,Ga)Se_2 thin films and solar cells. Ph.D. dissertation, Swiss Federal Institute of Technology, Zürich, 2004.
52. L.E. Oikkonen, M.G. Ganchenkova, A.P. Seitsonen, and R.M. Nieminen: Effect of sodium incorporation into $CuInSe_2$ from first principles. *J. Appl. Phys.* **114**, 083503 (2013).
53. B. Alling, H. Högberg, R. Armiento, J. Rosen, and L. Hultman: A theoretical investigation of mixing thermodynamics, age hardening potential, and electronic structure of ternary $M1_{1-x}M2_xB_2$ alloys with $A|B_2$ type structure. *Sci. Rep.* **5**, 09888 (2015).
54. N. Provatas and K. Elder: *Phase-Field Methods in Material Science and Engineering* (Wiley VCH, Singapore, 2010).
55. R.W. Balluffi, S.M. Allen, and W.C. Carter: *Kinetics of Materials* (John Wiley & Sons, Inc., Hoboken, NJ, USA, 2005).
56. H.P.C. Schaftenaar: *Theory and Examples of Spinodal Decomposition in a Variety of Materials* (Utrecht University, The Netherlands, 2008).
57. D.A. Porter, K.E. Easterling, and M.Y. Sherif: *Phase Transformations in Metals and Alloys*, 3rd ed. (CRC Press, Boca Raton FL, USA, 2009).
58. A.M. Holder, S. Siol, P.F. Ndione, H. Peng, A.M. Deml, B.E. Matthews, L.T. Schelhas, M.F. Toney, R.G. Gordon, W. Tumas, J.D. Perkins, D.S. Ginley, B.P. Gorman, J. Tate, A. Zakutayev, and S. Lany: Novel phase diagram behavior and materials design in heterostructural semiconductor alloys. *Sci. Adv.* **3**, e1700270 (2017).
59. J.W. Chan and R.J. Charles: The initial stages of phase separation in glasses. *Phys. Chem. Glasses* **6**, 181–191 (1965).
60. J. Sangster and A.D. Pelton: The Na–Se (sodium–selenium) system. *J. Phase Equilib.* **18**, 185–189 (1997).
61. J. Sangster and A.D. Pelton: The K–Se (potassium–selenium) system. *J. Phase Equilib.* **18**, 177–180 (1997).
62. J. Sangster and A.D. Pelton: The Rb–Se (rubidium–selenium) system. *J. Phase Equilib.* **18**, 190–193 (1997).
63. J. Sangster and A.D. Pelton: The Cs–Se (cesium–selenium) system. *J. Phase Equilib.* **18**, 173–176 (1997).
64. R. Hoppe, W. Lidecke, and F-C. Frorath: Zur Kenntnis von $NaInS_2$ und $NaInSe_2$. *Z. Anorg. Allg. Chem.* **309**, 49–54 (1961).
65. M. Schlosser, C. Reiner, H-J. Deiseroth, and L. Kienle: $K_2In_{12}Se_{19}$, a complex new structure type based on icosahedral units of Se^{2-}. *Eur. J. Inorg. Chem.* **2001**, 2241–2247 (2001).
66. G.E. Peterson and P.M. Bridenbaugh: Nuclear quadrupole coupling constants and charge distributions in ionic crystals of the $NaFeO_2$ type. *J. Chem. Phys.* **51**, 2610 (1969).

https://doi.org/10.1557/jmr.2017.394 Published online by Cambridge University Press

67. B. Krebs: Thio- und Selenoverbindungen von Hauptgruppenelementen–neue anorganische Oligomere und Polymere. *Angew. Chem.* **95**, 113–134 (1983).
68. F.Q. Huanga, B. Denga, D.E. Ellis, and J.A. Ibers: Preparation, structures, and band gaps of $RbInS_2$ and $RbInSe_2$. *J. Solid State Chem.* **178**, 2128–2132 (2005).
69. J. Do and M.G. Kanatzidis: The one-dimensional polyselenide compound $CsGaSe_3$. *Z. Anorg. Allg. Chem.* **629**, 621–624 (2003).
70. D. Friedrich, M. Schlosser, and A. Pfitzner: Synthesis and structural characterization of $Cs_2Ga_2Se_5$. *Z. Anorg. Allg. Chem.* **640**(5), 826–829 (2014).
71. M.B. Zellner, R.W. Birkmire, E. Eser, W.N. Shafarman, and J.G. Chen: Determination of activation barriers for the diffusion of sodium through CIGS thin-film solar cells. *Prog. Photovoltaics* **11**, 543–548 (2003).
72. J-H. Yoon, T-Y. Seong, and J. Jeong: Effect of a Mo back contact on Na diffusion in CIGS thin film solar cells. *Prog. Photovoltaics* **21**, 58–63 (2013).
73. A. Laemmle, R. Wuerz, T. Schwarz, O. Cojocaru-Mirédin, P.P. Choi, and M. Powalla: Investigation of the diffusion behavior of sodium in Cu(In,Ga)Se_2 layers. *J. Appl. Phys.* **115**, 154501 (2014).
74. D. Abou-Ras, S.S. Schmidt, R. Caballero, T. Unold, H-W. Schock, C.T. Koch, B. Schaffer, M. Schaffer, P-P. Choi, and O. Cojocaru-Mirédin: Confined and chemically flexible grain boundaries in polycrystalline compound semiconductors. *Adv. Energy Mater.* **2**, 992–998 (2012).
75. P.P. Choi, O. Cojocaru-Mirédin, R. Wuerz, and D. Raabe: Comparative atom probe study of Cu(In,Ga)Se_2 thin-film solar cells deposited on soda-slime glass and mild steel substrates. *J. Appl. Phys.* **110**, 124513 (2011).
76. M.A. Contreras, B. Egaas, P. Dippo, J. Webb, J. Granata, K. Ramanathan, S. Asher, A. Swartzlander, and R. Noufi: On the role of Na and modifications to Cu(In,Ga)Se_2 absorber materials using thin MF (M = Na, K, Cs) precursor layers. In *Rec. 26th IEEE Photovoltaic Spec. Conf., Anaheim, California, September 29-October 3* (IEEE, New York, 1997); pp. 359–362.
77. Database of the International Centre for Diffraction Data, JCPDS 01-074-0136.
78. Y.C. Lin, Z.H. Shi, C.H. Shen, and Y.L. Chen: Na-doped Mo target sputtering for CIGS thin film solar cells on stainless steel substrate. *Int. J. Appl. Phys. Math.* **3**, 157–160 (2013).
79. J.W. Lee, R. Kaczynski, J. Van Alsburg, B. Sang, U. Schoop, and J. Britt: Effect of three-stage growth modification on a CIGS microstructure. *IEEE J. Photovolt.* **6**, 1645–1649 (2016).
80. V. Nadenau, G. Lippold, U. Rau, and H.W. Schock: Sodium induced secondary phase segregations in $CuGaSe_2$ thin films. *J. Cryst. Growth* **233**, 13–21 (2001).
81. M.R. Balboul, M. Turcu, I.M. Kötschau, U Rau, and H.W. Schock: Sodium induced phase segregations in $CuGaSe_2$ and $CuInSe_2$ thin films. In *Proc. 17th Eur. Photovoltaic Sol. Energy Conf., Munich Germany, October 22–26*, B. McNelis, W. Palz, H.A. Ossenbrink, and P. Helm, eds. (WIP, Munich, Germany, 2001); pp. 1015–1018.
82. X. Song, R. Caballero, R. Félix, D. Gerlach, C.A. Kaufmann, H-W. Schock, R.G. Wilks, and M. Bär: Na incorporation into Cu(In,Ga)Se_2 thin-film solar cell absorbers deposited on polyimide: Impact on the chemical and electronic surface structure. *J. Appl. Phys.* **111**, 034903 (2012).
83. D. Schmid, M. Ruckh, F. Grunwald, and H.W. Schock: Chalcopyrite defect chalcopyrite heterojunctions on the basis of $CuInSe_2$. *J. Appl. Phys.* **73**, 2902 (1993).
84. M.A. Contreras and R. Noufi: Chalcopyrite Cu(In,Ga)Se_2 and defect-chalcopyrite Cu(In,Ga)$_3Se_5$ materials in photovoltaic P–N junctions. *J. Cryst. Growth* **174**, 283–288 (1997).
85. H. Mönig, C-H. Fischer, A. Grimm, B. Johnson, C.A. Kaufmann, and R. Caballero: Surface Cu-depletion of Cu(In,Ga)Se_2 thin films: Further experimental evidence for a defect-induced surface reconstruction. *J. Appl. Phys.* **107**, 113540 (2010).
86. P. Reinhard, B. Bissig, F. Pianezzi, H. Hagendorfer, G. Sozzi, R. Menozzi, C. Gretener, S. Nishiwaki, S. Buecheler, and A.N. Tiwari: Alkali-templated surface nanopatterning of chalcogenide thin films: A novel approach toward solar cells with enhanced efficiency. *Nano Lett.* **15**, 3334–3340 (2015).
87. E. Handick, P. Reinhard, R.G. Wilks, F. Pianezzi, R. Félix, M. Gorgoi, T. Kunze, S. Buecheler, A.N. Tiwari, and M. Bär: NaF/KF post-deposition treatments and their influence on the structure of Cu(In,Ga)Se_2 absorber surfaces. In *Rec. 43rd IEEE Photovoltaic Spec. Conf., Portland, Oregon, June 5–6* (IEEE, New York, 2016); pp. 017–021.
88. M. Malitckaya, H-P. Komsa, V. Havu, and M. Puska: Effect of alkali metal atom doping on $CuInSe_2$-based solar cell absorber. *J. Phys. Chem. C* **121**, 15516–15528 (2017).
89. F. Couzinie-Devy, E. Cadel, N. Barreau, L. Arzel, and P. Pareige: Atom probe study of Cu-poor to Cu-rich transition during Cu(In,Ga)Se_2 growth. *Appl. Phys. Lett.* **99**, 232108 (2011).
90. G. Hanna: Determination and influence of Na supply and Se flux during growth of Cu(In,Ga)Se_2 thin films. Ph.D. dissertation, University of Stuttgart, Germany, 2004.
91. D. Colombara, U. Berner, A. Ciccioli, J.C. Malaquias, T. Bertram, A. Crossay, M. Schöneich, H.J. Meadows, D. Regesch, S. Delsante, G. Gigli, N. Valle, J. Guillot, B.E. Adib, P. Grysan, and P.J. Dale: Deliberate and accidental gas-phase alkali doping of chalcogenide semiconductors: Cu(In,Ga)Se_2. *Sci. Rep.* **7**, 43266 (2017).
92. Z.K. Yuan, S. Chen, Y. Xie, J.S. Park, H. Xiang, X.G. Gong, and S.H. Wei: Na-diffusion enhanced p-type conductivity in Cu(In,Ga)Se_2: A new mechanism for efficient doping in semiconductors. *Adv. Energy Mater.* **6**, 1601191 (2016).

https://doi.org/10.1557/jmr.2017.394 Published online by Cambridge University Press